Available online at www.sciencedirect.com

ScienceDirect

Procedia Structural Integrity 38 (2022) 519–525

Structural Integrity Procedia

www.elsevier.com/locate/procedia

FATIGUE DESIGN 2021, 9th Edition of the International Conference on Fatigue Design

# A Comparative Study on Fatigue Performance of Various Additively Manufactured Titanium Alloys

Mohammad Salman Yasin[a,b], Arash Soltani-Tehrani[a,b], Shuai Shao[a,b], Meysam Haghshenas[c], Nima Shamsaei[a,b,*]

[a]*Department of Mechanical Engineering, Auburn University, Auburn, AL 36849, USA*
[b]*National Center for Additive Manufacturing Excellence (NCAME), Auburn University, Auburn, AL 36849, USA*
[c]*Department of Mechanical, Industrial, and Manufacturing Engineering, University of Toledo, Toledo, OH 43606, USA*

**Abstract**

Titanium alloys have been used extensively in aerospace and medical applications due to their exceptional strength to weight ratio, biocompatibility, and corrosion resistance. While these alloys are known to be difficult to machine, they are typically weldable. Therefore, various titanium-based alloys have been recently considered for production via additive manufacturing technology. Additively manufactured titanium alloys are used to produce a wide range of high-performance components, which are often under cyclic or periodic loading. While the most commonly used titanium alloy (i.e. Ti-6Al-4V) has been extensively characterized, there is a gap in the literature with regards to the fatigue performance of many other titanium alloys considered for additive manufacturing. This study aims at assessing the microstructural, mechanical, and fatigue performance of two additively manufactured titanium-based alloys, Ti-5Al-5V-5Mo-3Cr and Ti-5Al-5Mo-5V-1Cr-1Fe, and comparing the results with the ones for the well-studied Ti-6Al-4V. An EOS M290 laser beam powder bed fusion (LB-PBF) additive manufacturing machine is used to fabricate specimens from various titanium alloys for this study. Specimens are characterized and compared side by side for their porosity, microstructure, tensile, and fatigue behavior.



*Keywords:* Additive manufacturing; Laser beam powder bed fusion; Fatigue; Titanium alloys; Ti-5553; Ti-55511; Ti-64

* Corresponding author. Tel: +1-334-844-4839
*E-mail address: shamsaei@auburn.edu*


10.1016/j.prostr.2022.03.052

## 1. Introduction

The good strength to weight ratio, biocompatibility, and high corrosion resistance make titanium alloys appealing as compared to other conventional metals such as aluminum, steel, etc (Joshi, 2006; Sha & Malinov, 2009). However, these alloys are usually difficult to machine due to their high chemical reactivity, low modulus of elasticity, and low thermal conductivity (Khanna and Davim (2015); Pramanik (2014)) This illustrates that the application of such alloys hangs in balance due to the high machining cost, which would reduce as the need for machining decreases.

Among the various near-net-shape techniques, additive manufacturing (AM) has become popular for fabricating titanium alloys. However, of all titanium alloys, the majority still leans towards the workhorse of the titanium industry, Ti-6Al-4V (Ti-64), an alpha-beta phase titanium alloy (Lütjering and Williams (2007)). As such, researchers have extensively studied the behavior of Ti-64. The current paper aims to focus on two near beta titanium alloys, Ti-5Al-5V-5Mo-3Cr (Ti-5553) and Ti-5Al-5Mo-5V-1Cr-1Fe (Ti-55511).

Ti-5553 is built based on the Ti-alloy Ti-55511 (also known as VT22) and was announced by Titanium Metals Cooperation (Bartus (2009); Jones et al. (2009)). Both alloys present a wide range of mechanical properties due to the prospect of modifying the two-phase microstructure through thermo-mechanical treatments (Clément, 2010; Kolli & Devaraj, 2018; Schwab et al., 2017). This has helped Ti-5553 replace Ti-10V-2Fe-3Al in structural components for the landing gear of Boeing airframes.

The objective of the present study is to assess the microstructural and mechanical behavior (such as tensile and fully reversed fatigue behavior) of Ti-5553 and Ti-55511 fabricated using laser beam powder bed fusion (LB-PBF), a powder-based AM technology, and to make a comparison with the Ti-64 counter material. The conducted study used specimens, which were fabricated by an EOS M290 machine using the same process parameters in a vertical orientation and later machined to required geometry based on ASTM standards. In the following sections, the experimental setup is discussed along with the results and discussion.

## 2. Experimental setup

In this study, two near-beta titanium alloys, Ti-5553 and Ti-55511 were investigated. The LB-PBF system used for fabricating the specimens was an EOS M290 and the powders used as feedstock were supplied by AP&C, a GE Additive company. The process parameters used for the fabrications were kept the same for both materials. The infill parameters were 280W laser power, 1200 mm/s scan speed, 140 μm hatch distance, 30 μm layer thickness, and 67° hatch rotation. This yielded an energy density of 55.6 J/mm$^3$. The build layouts for AM fabrication were also kept similar and can be seen in Fig 1. Some specimens were not fabricated due to complications during manufacturing. Round bars of 13 mm diameter and 100 mm height were fabricated and later shaped into tensile and fatigue specimens according to ASTM E8 and E466 respectively (ASTM International (2015), (2021)). Some net-shaped fatigue specimens were also fabricated with side support to obtain the fatigue behavior of the materials in the as-built surface condition. Additionally, eight half-built specimens were placed in different locations of the build plate for microstructural analysis.

After fabrication, the specimens were taken off of the build plate and some half-built, tensile, and fatigue specimens were stress-relieved at 900°C in an inert (argon) atmosphere for an hour and then furnace-cooled to room temperature. Microstructural characterization of the LB-PBF titanium alloys along the build direction was studied in the non-heat-treated (NHT) condition to reveal the melt-pool morphologies obtained during the fabrication. The melt-pools were revealed using a modified Kroll's reagent (10% HF, 10% $HNO_3$, and 80% distilled water) and analyzed using a Keyence VHX-6000.

To obtain the relative density and overall defect distribution of the fabricated specimens, at least two machined specimens were scanned for X-ray computed tomography (XCT) using a Zeiss Xradia 620 versa machine at 0.4X magnification. The voltage and current used for the analysis under 0.4X magnification were 140 kV and 150 μA respectively. The alignment of the detector and source were changed within the X-ray machine to obtain a resolution of 6 μm voxel size. This would indicate that the minimum feature size that the scan could detect would be 6 μm in size. The resulting images were post-processed using the Scout and Reconstruct software. ImageJ was used to analyze the defect size distribution. However, to account for any noises, volumes less than 525 μm$^3$ (equivalent diameter of 10 μm) were discarded from the analysis.

**Nomenclature**

| | |
|---|---|
| AM | Additive manufacturing |
| Ti-64 | Ti-6Al-4V |
| Ti-5553 | Ti-5Al-5V-5Mo-3Cr |
| Ti-55511 | Ti-5Al-5Mo-5V-1Cr-1Fe |
| LB-PBF | Laser beam powder bed fusion |
| NHT | Non-heat-treated |
| XCT | X-ray computed tomography |
| $\sigma_a$ | Stress amplitude |
| $2N_f$ | Number of reversals to failure |
| E | Young's modulus |
| $S_u$ | Ultimate tensile strength |
| %EL | Percent elongation to failure |

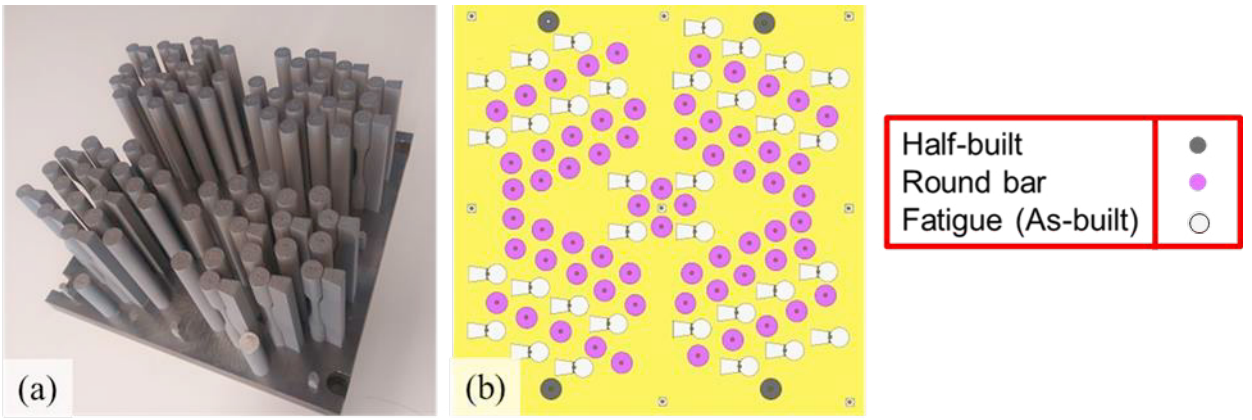


Figure 1: (a) Representative build plate after fabrication and (b) top view of the fabricated build layout

Quasi-static tensile properties were evaluated using 12-mm gauge length round machined specimens at ambient temperature employing an MTS landmark servo-hydraulic testing machine with 100 kN load cells. To calculate the yield strength of the materials accurately, an extensometer was used to measure strain up to 0.05 mm/mm strain at 0.001 mm/mm.s strain rate. Next, the extensometer was removed and the test was continued until failure on displacement-control mode. Fatigue tests were performed under fully reversed (stress ratio, $R = \sigma_{min}/\sigma_{max} = -1$) condition. All fatigue tests were conducted under force-controlled conditions via a 25-kN servo-hydraulic MTS machine and at least three specimens were tested at each stress level. The fatigue tests were continued until failure with a sinusoidal loading control.

## 3. Result and discussion

### *3.1. Microstructural analysis*

To understand the variability arising from the different titanium alloys: Ti-5553 and Ti-55511, the melt pool morphology was taken into account. Fig. 2 shows the optical micrographs (OMs) of the top layers of the polished and etched half-built samples. Few of the elliptical-shaped melt-pools are highlighted using yellow dashed lines. A methodology according to NASA MSCF 3717 indicated that the ratios between the melt-pool depth ($d_p$) and layer thickness ($t$), and also between the overlap depth ($d_o$) to layer thickness can be used as a characteristic tool to identify

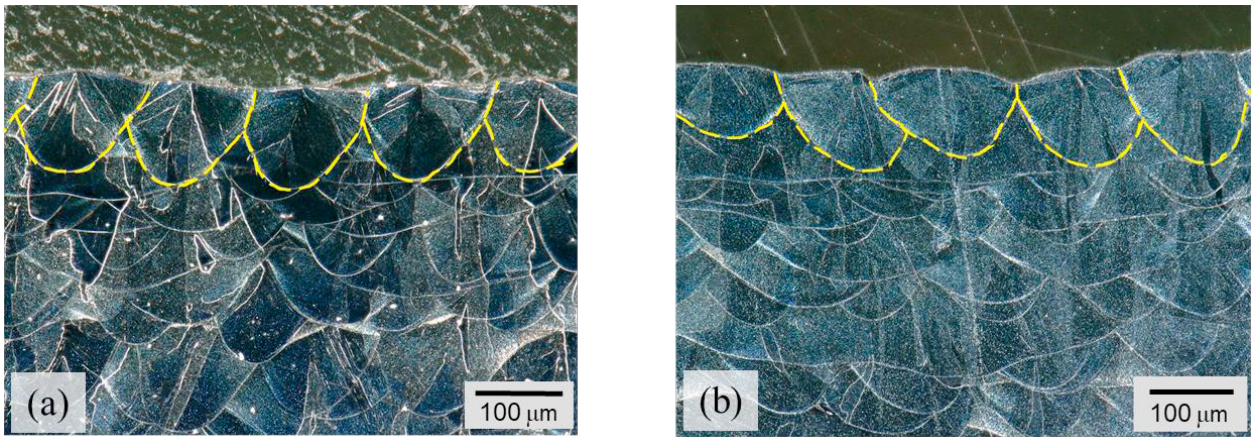


Figure 2: Melt pools at the top surface of (a) Ti-5553 and (b) Ti-55511 specimens after fabrication

the process health (NASA (2017)). The ratio $d_p/t$ indicates the likelihood of defects such as gas entrapped pores, and on the other hand, the $d_o/t$ is indicative of the formation of defects such as lack of fusion. The $d_0/t$ and $d_p/t$ ratios for Ti-5553 were 1.5 and 4 respectively; on the other hand, the ratios were found as 1.7 and 3.9 respectively for Ti-55511. Thus, there is a possibility of forming more smaller gas pores during the fabrication of Ti-5553 as the small $d_0/t$ value indicates a higher probability of forming gas pores (Nezhadfar et al., 2021; Shrestha et al., 2019; Soltani-Tehrani, Shrestha, et al., 2021).

### *3.2. Porosity analysis*

Non-destructive testing such as X-ray tomography is often used to analyze the internal defect morphology of the specimens. A gauge section of 5 mm in height of the machined specimens was scanned for XCT analysis. The XCT analysis revealed an average relative density of 99.993% and 99.994% for Ti-5553 and Ti-55511 respectively. Fig. 3

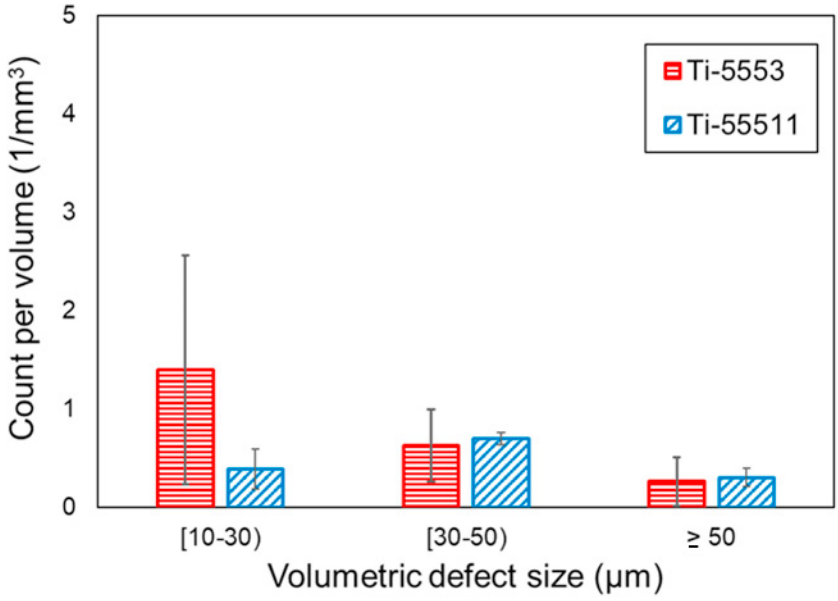


Figure 3: Pore size distribution for Ti-5553 and Ti-55511

illustrates the pore size distribution obtained through XCT analysis for both titanium alloys. The results show that there are larger size pores in Ti-55511 specimens in comparison to a larger number of smaller size pores in Ti-5553. The largest defect of equivalent diameter detected from the analysis for both materials was 94 and 89 µm and also the average diameter was found to be 27 and 39 µm, respectively.

### *3.3. Tensile behavior*

A representation of the quasi-static tensile behavior of the two titanium alloys is shown in Fig. 4 in terms of stress-displacement curves from the start of the test until failure. The ultimate tensile strength ($S_u$), Young's modulus ($E$), and percent elongation to failure (%EL) of the alloys have been compared to that of wrought and additively manufactured Ti-64 and are presented in Table 1. Since two specimens of each alloy were tested, the average values have been indicated in the table. Both the Ti-5553 and Ti-55511 presented higher $S_u$ in comparison to wrought and AM Ti-64 (Carrion et al. (2017); Soltani-Tehrani et al. (2021)). However, in terms of *%EL* and *E*, both alloys are comparable. The equivalent ductility can be attributed to the almost similar porosity level of the fabricated specimens.

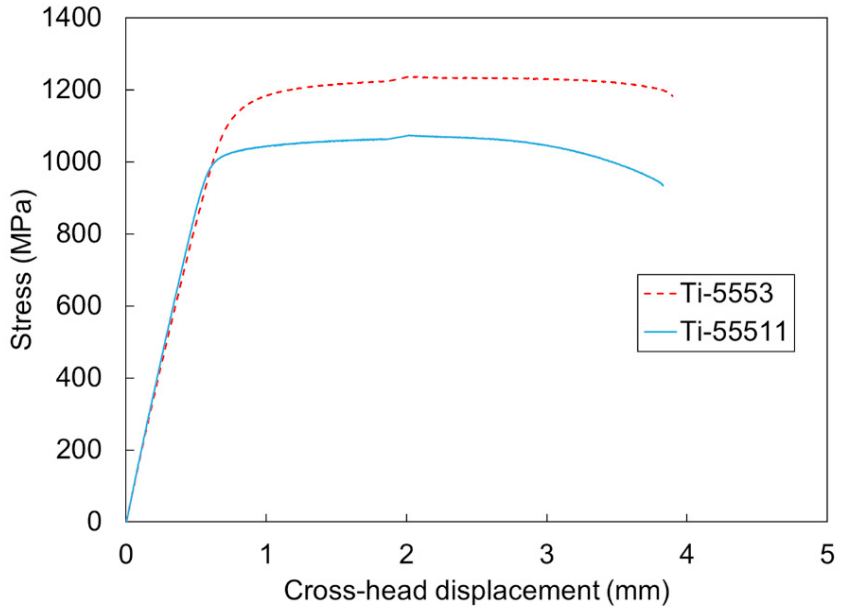


Figure 4: Quasi-static tensile behavior of Ti-5553 and Ti-55511

Table 1. Tensile properties of various titanium alloys including Ti-5553, Ti-55511, and Ti-64 processed with AM and compared with the wrought Ti-64 (Carrion et al. (2017); Soltani-Tehrani et al. (2021)).

| Alloy | $S_u$ (MPa) | E (GPa) | %EL |
|---|---|---|---|
| Ti-5553 (LB-PBF) | 1213.1 ± 7.6 | 111.0 ± 0.6 | 15.5 ± 0.1 |
| Ti-55511 (LB-PBF) | 1105.1 ± 18.4 | 110.6 ± 3.4 | 14.6 ± 3.9 |
| Ti-64 (LB-PBF) | 1018.0 ± 3.0 | 116.8± 0.5 | 17.0 ± 0.0 |
| Ti-64 (Wrought) | 1062 | 106 | 15 |

### *3.4. Fatigue behavior*

Figure 5 illustrates a semi-log plot of stress amplitude versus reversals to failure of LB-PBF titanium alloys in comparison to LB-PBF Ti-64 specimens. From Fig. 5, it can be seen that for the three stress levels tested (i.e., 400, 500, and 700 MPa), Ti-5553 outperformed Ti-55511 slightly in terms of average reversals to fatigue failure. For most cases, the crack initiation of the fatigue specimens happened due to defects close to the surface, which is quite common for additively manufactured parts. Moreover, in comparison to the fatigue life of AM Ti-64 found in the literature (Soltani-Tehrani et al. (2021)), it can be seen that, in low cycle fatigue regime (i.e., 700 MPa), there is a comparable difference between the average life of the specimens which can be attributed to the lower ductility of Ti-5553 in comparison to Ti-64. On the other hand, in the High cycle fatigue (HCF) regime (i.e., 400 MPa), all three materials performed almost similar in terms of average fatigue life. The variation within the specimens' fatigue lives can be attributed to the number, size, and location of defects present within the specimens since, in the HCF, the near-to-surface defects can cause localized stress concentration, even with loading in the elastic region (Molaei et al. (2020); Yadollahi et al. (2015)).

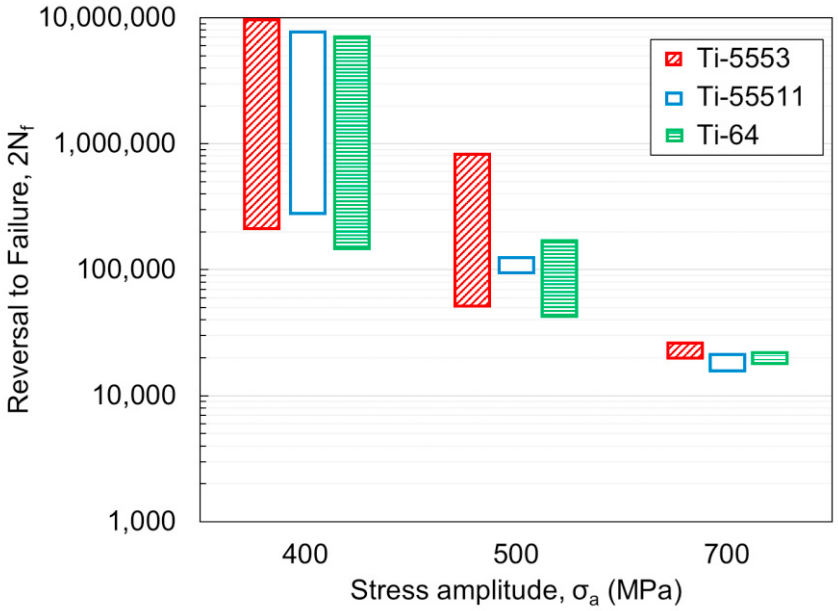


Figure 5: : Fatigue life range obtained for different additively manufactured titanium alloys including Ti-5553, Ti-55511, and Ti-64

## 4. Conclusion

In this study, the tensile and fatigue performance of two additively manufactured near-beta titanium alloys including Ti-5553 and Ti-55511 were studied in comparison to that of Ti-64. The experimental results illustrated that it is feasible to tailor the microstructure and part performance of AM parts as desired by modifying some specific alloying elements in the titanium alloys, which in turn resulted in some improvement in the tensile and fatigue performance of additively manufactured parts. In addition, some conclusions were made based on the experimental observations as follow:

- The microstructure in the NHT condition for both alloys was similar, due to the use of the same process parameters and similar build layouts.

- Although Ti-5553 showed higher tensile strength, the elongation of both alloys was comparable to that of AM and wrought Ti-64.
- A slight difference was observed in the fatigue lives of the compared three alloys. However, the presented data had a significant amount of scattering, which needs to be addressed with further testing.

## Acknowledgments

This material is based upon work supported by the National Institute of Standards and Technology, under Award Number # 70NANB17H295.

## References

ASTM International. (2015). *ASTM E466-15, Standard Practice for Conducting Force Controlled Constant Amplitude Axial Fatigue Tests of Metallic Materials*. www.astm.org

ASTM International. (2021). *ASTM E8 / E8M-21, Standard Test Methods for Tension Testing of Metallic Materials*. www.astm.org

Bartus, S. D. (2009). Evaluation of Titanium-5Al-5Mo-5V-3Cr (Ti-5553 ) Alloy Against Fragment and Armor-Piercing Projectiles. *ARL-TR-4996*.

Carrion, P. E., Shamsaei, N., Daniewicz, S. R., & Moser, R. D. (2017). Fatigue behavior of Ti-6Al-4V ELI including mean stress effects. *International Journal of Fatigue*, *99*, 87–100.

Clément, N. (2010). *Phase transformations and mechanical properties of the Ti-5553 β-metastable titanium alloy*. 314 p. http://hdl.handle.net/2078.1/32266

Jones, N. G., Dashwood, R. J., Jackson, M., & Dye, D. (2009). β Phase decomposition in Ti-5Al-5Mo-5V-3Cr. *Acta Materialia*. https://doi.org/10.1016/j.actamat.2009.04.031

Joshi, V. A. (2006). *Titanium alloys: an atlas of structures and fracture features*. Crc Press.

Khanna, N., & Davim, J. P. (2015). Design-of-experiments application in machining titanium alloys for aerospace structural components. *Measurement: Journal of the International Measurement Confederation*, *61*, 280–290. https://doi.org/10.1016/j.measurement.2014.10.059

Kolli, R. P., & Devaraj, A. (2018). A review of metastable beta titanium alloys. In *Metals*. https://doi.org/10.3390/met8070506

Lütjering, G., & Williams, J. C. (2007). *Titanium*. Springer Science & Business Media.

Molaei, R., Fatemi, A., Sanaei, N., Pegues, J., Shamsaei, N., Shao, S., Li, P., Warner, D. H., & Phan, N. (2020). Fatigue of additive manufactured Ti-6Al-4V, Part II: The relationship between microstructure, material cyclic properties, and component performance. *International Journal of Fatigue*, *132*, 105363. https://doi.org/10.1016/j.ijfatigue.2019.105363

NASA. (2017). *MSFC-SPEC-3717 | NASA Technical Standards System (NTSS)* (p. 58). https://standards.nasa.gov/standard/msfc/msfc-spec-3717

Nezhadfar, P. D., Shamsaei, N., & Phan, N. (2021). Enhancing ductility and fatigue strength of additively manufactured metallic materials by preheating the build platform. *Fatigue & Fracture of Engineering Materials & Structures*, *44*(1), 257–270.

Pramanik, A. (2014). Problems and solutions in machining of titanium alloys. *International Journal of Advanced Manufacturing Technology*, *70*(5–8), 919–928. https://doi.org/10.1007/s00170-013-5326-x

Schwab, H., Bönisch, M., Giebeler, L., Gustmann, T., Eckert, J., & Kühn, U. (2017). Processing of Ti-5553 with improved mechanical properties via an in-situ heat treatment combining selective laser melting and substrate plate heating. *Materials and Design*. https://doi.org/10.1016/j.matdes.2017.05.010

Sha, W., & Malinov, S. (2009). *Titanium alloys: modelling of microstructure, properties and applications*. Elsevier.

Shrestha, R., Shamsaei, N., Seifi, M., & Phan, N. (2019). An investigation into specimen property to part performance relationships for laser beam powder bed fusion additive manufacturing. *Additive Manufacturing*, *29*, 100807. https://doi.org/https://doi.org/10.1016/j.addma.2019.100807

Soltani-Tehrani, A., Shrestha, R., Phan, N., Seifi, M., & Shamsaei, N. (2021). Establishing Specimen Property to Part Performance Relationships for Laser Beam Powder Bed Fusion Additive Manufacturing. *International Journal of Fatigue*.

Soltani-Tehrani, A., Yasin, M. S., Habibnejad, M., Haghshenas, M., & Shamsaei, N. (2021). Effects of Powder Particle Size on Fatigue Performance of Laser Powder-Bed Fused Ti-6Al-4V. *Fatigue Design 2021*.

Yadollahi, A., Shamsaei, N., Thompson, S. M., & Seely, D. W. (2015). Effects of process time interval and heat treatment on the mechanical and microstructural properties of direct laser deposited 316L stainless steel. *Materials Science and Engineering: A*, *644*, 171–183.